Impact of Power Flow Direction on the Stability of VSC-HVDC Seen From the Impedance Nyquist Plot

Mohammad Amin, *Member, IEEE*, Marta Molinas, *Member, IEEE*, Jing Lyu, *Student Member, IEEE*, and Xu Cai

***Abstract*—The high-voltage dc (HVDC) systems are appearing more and more, and it is becoming a requirement that the HVDC voltage-source converters (VSCs) operate both as an inverter and a rectifier without changing the controls to provide the flexibility of having power flows in both directions. It is observed that the HVDC system operates stably when the power flow direction is from the power-controlled converter to the dc-voltage-controlled converter, and it becomes unstable when the power flow direction has been altered. In order to analyze such an instability problem and to design the local control, an impedance-based method is proposed. Identifying the source and the load impedance are prerequisite to apply the impedance-based method. The existing method of determining the source and the load impedance cannot predict the stability when the power flow direction is altered; therefore, a method based on the power flow direction has been presented to determine the source and the load impedance. The converter that injects power to the dc system is the current source represented with its Norton equivalent parallel impedance, while the other converter impedance is considered as the load impedance. The stability of the system is determined by the ratio of the load impedance to the current-source impedance. Once the source and the load impedance are analytically obtained, the impedance-based Generalized Nyquist stability criterion is applied to determine the stability. The system stability for the two power flow directions is well predicted from the Nyquist plot of impedance ratio. A two-terminal HVDC system has been developed in MATLAB/Simulink to demonstrate the application of this method, and the results are compared with the experimental results.**

***Index Terms*—High-voltage dc (HVDC), impedance analysis, Nyquist stability criteria, power flow direction, stability analysis, voltage-source converter (VSC) control.**

I. Introduction

THE voltage-source converter (VSC)-based high-voltage dc (HVDC) transmission system has received considerable attention due to development of the power electronics converter [1], [2]. A large range of modeling and control of the VSC-based HVDC system have been published in the last few years [3]–[11]. From these studies, it becomes clear that the control and the system impedance can have the impact on the stability of the system. It is, therefore, necessary to preassess their impact on the system stability before connecting to the main grid. Continuous efforts have been made to investigate the stability of such a system by different approaches. Existing approaches for the stability study of the VSC-HVDC system are based on the controller dynamics that do not include the system impedance and the dc-line dynamics. Another approach is based on the state-space model and eigenvalue analysis [12]–[18]. The eigenvalue-based approach requires the design of each components of the HVDC system and does not support the local control development at individual terminals. The impedance-based approach is a simple method for stability analysis and supports the local control development [19]–[34].

A common practice when designing the control of an HVDC is: the dc-voltage-controlled converter operates as an inverter and the power-controlled converter operates as a rectifier [35]. Thus, the active power flows in one direction from the power control to the dc-voltage-controlled converter. If it is necessary to change the power flow direction, the control mode between the converters needs to be changed. However, the HVDC systems are appearing more and more, and it is becoming a requirement that the VSCs operate both as an inverter and a rectifier without changing the controls to provide the flexibility of having power flows in both directions [36], as an ac transmission system in which two ac networks support each other. It has been observed that the HVDC system operates stably when the power flow direction is from the power-controlled converter to the dc-voltage-controlled converter, and it becomes unstable when the power flow direction has been altered. The existing impedance-based stability method cannot determine the stability when the power flow direction has been altered. This paper has proposed a method based on the impedances Nyquist plot to investigate such an instability problem.

In order to determine the stability based on the impedance-based approach, the impedance model derivation is the prerequisite. In the literature, most researchers have so far focused on the ac impedance modeling either in the positive–negative sequence [26], [27] or in the dq frame [28]–[31] and considered to have an ideal voltage source or a current source in the dc side, in which the dc lines/cables impedance are neglected. However, in a VSC-based HVDC system the dc-side dynamics have a significant impact on the system stability. Therefore,

Manuscript received June 3, 2016; revised July 28, 2016; accepted September 7, 2016. Date of publication September 9, 2016; date of current version May 9, 2017. The Ph.D. studies of M. Amin are partly supported by the project Protection and Fault Handling in Offshore HVDC Grids (ProOfGrids), managed by SINTEF Energy Research and financed by the Norwegian Research Council together with industry partners: EDF, NVE, National Grid, Siemens, Statkraft, Statnett, and Statoil. Recommended for publication by Associate Editor F. Fuchs.

M. Amin and M. Molinas are with the Department of Engineering Cybernetics, Norwegian University of Science and Technology, 7491 Trondheim Norway (e-mail: mohammad.amin@ntnu.no; marta.molinas@ntnu.no).

J. Lyu and X. Cai are with the Wind Power Research Center, Shanghai Jiao Tong University, Shanghai 200240, China (e-mail: lvjing@sjtu.edu.cn; xucai@sjtu.edu.cn).

Color versions of one or more of the figures in this paper are available online at http://ieeexplore.ieee.org.

Digital Object Identifier 10.1109/TPEL.2016.2608278

the impact of the dc-line impedance must be considered in the stability analysis. A dc-impedance-based resonance analysis for the VSC-HVDC system is investigated for different values of the dc-link capacitance in [35]; however, it does not include the detailed stability analysis. Another dc-impedance-based stability method has been presented in [22] and [24]; however, these papers have not discussed the impact of the power flow direction on the stability.

In this study, a dc-impedance-based approach is adopted to analyze the stability of the VSC-based HVDC transmission system. An analytical method is derived to calculate the dc impedance, which refers to the impedance of the VSC including the controller dynamics and the dc-line impedance. The derived model is validated by comparing the frequency response of the analytical impedance and the impedance measured at the dc terminal from a detailed switching model of the VSC-HVDC system. The impedance of the VSCs not only depends on the passive components, but also on the converter control dynamics.

In order to apply the impedance-based stability method, it is necessary to determine the source and the load impedances. A method for determining the current source and the voltage source for the dc system has been presented in [37], in which the subsystem connected in series with an inductor is assumed to be the current source, while the converter connected in parallel with a capacitor is assumed to be the voltage source. Moreover, in the literature, the subsystem that regulates the voltage is assumed to be the voltage source, and other converter is assumed to be the current source regardless of the direction of the current (power flow) [20]. Hence, the system can be represented by an equivalent small-signal impedance model consisting of both the voltage source and the current source, and the stability can be determined from the minor loop gain, which is the ratio of the voltage-source to the current-source impedance [20]. However, the stability of a system consisting of a current-source and a voltage-source system cannot be determined for both directions of the active power flow. A method based on the generalized inverse Nyquist criteria (GINC) has been presented in [29], which could be useful to analyze such an instability problem, but it does not have any indication when should be used the generalized Nyquist criteria (GNC) or GINC for a case when the power flow direction has been altered.

It is, therefore, important to design the control, which makes the system stable for both directions of power flow. To design the appropriate control, the instability problem needs to be defined analytically. In an attempt to do that, an impedance-based method is proposed, and the HVDC converter stations are represented by its Norton equivalent current source with parallel-connected impedance, and the source and the load impedance are determined based on the power flow direction. The identification of the source and the load impedance is based on the power flow direction, which is a new method presented in this paper. The stability analysis has been performed for two different directions of power flow, where the method can determine the stability for both directions of power flow and the theoretical analysis has been verified by time-domain simulation and by experiments.

The rest of this paper is organized as follows: Section II describes the modeling and control of the HVDC system. The developed HVDC system is tested by time-domain simulation and experiment in Section III. Section IV presents the impedance-based stability method. Moreover, an impedance model is derived analytically and the derived impedance model is verified with the frequency response of the impedance obtained from simulation. The stability analysis method based on the power flow direction is described in Section V. Finally, the results of this study are concluded in Section VI.

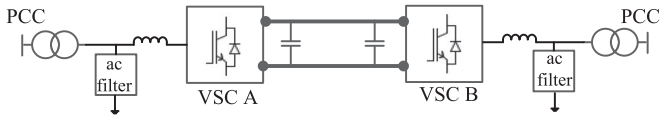

Fig. 1. Point-to-point connection VSC-based HVDC system.

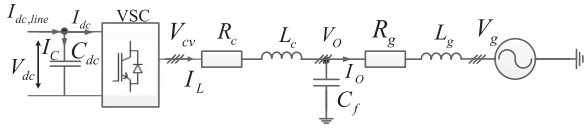

Fig. 2. Overview of VSC-HVDC converter station.

II. HVDC System Modeling and Control

The two-terminal VSC-based HVDC system under this study is depicted in Fig. 1. The HVDC system consists of the converter transformers, ac filters, two VSC HVDC converters named VSC-A and VSC-B, and the dc cable. Both the VSC-A and VSC-B are assumed to be identical in structure. The electrical circuit of a VSC-HVDC converter for analytical modeling is shown in Fig. 2, where L_c and R_c are the total series inductance and resistance of the VSC, C_f is the filter capacitance, and L_g and R_g are the inductance and resistance of the grid. The modeling, analysis, and control of the system will be presented in a synchronous reference frame (SRF). The transformation of the three-phase quantity from stationary reference frame to the SRF is based on the amplitude-invariant Park transformation, with the d-axis aligned with the voltage vector v_o and q-axis leading the d-axis by 90°. The dynamic equations of the converter in per unit (p.u.) can be given by (1), the filter by (2), and the grid by (3), where ω_b is the base angular grid frequency, ω_g is the grid frequency in p.u., and voltage and current of these equations are indicated in Fig. 2 [38], [39]

$$\frac{di_L}{dt} = \frac{\omega_b}{L_c} v_{\rm cv} - \frac{\omega_b}{L_c} v_o - \omega_b \left(\frac{R_c}{L_c} + j\omega_g \right) i_L \tag{1}$$

$$\frac{dv_o}{dt} = \frac{\omega_b}{C_f} i_L - \frac{\omega_b}{C_f} i_o - j\omega_b \omega_g v_o \tag{2}$$

$$\frac{di_o}{dt} = \frac{\omega_b}{L_g} v_o - \frac{\omega_b}{L_g} v_g - \omega_b \left(\frac{R_g}{L_g} + j\omega_g \right) i_o. \tag{3}$$

A. Current Controller

The inner-loop current controller is assumed to be the widely used SRF proportional-integral (PI) controller of the VSC with a decoupling term. The output voltage references $v_{cvdq,ref} = \begin{pmatrix} v_{cvd,ref} & v_{cvq,ref} \end{pmatrix}^T$ obtained from the current controller

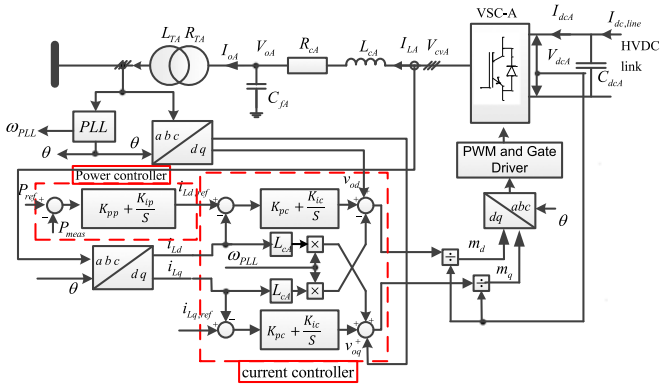

Fig. 3. Control structure of the power-controlled converter.

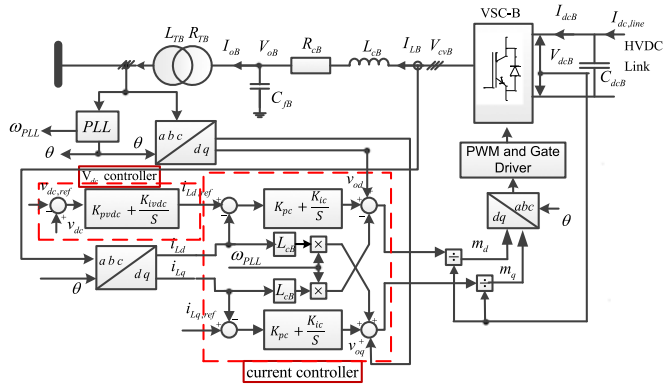

Fig. 4. Control structure of the dc-voltage-controlled converter.

including the feedforward terms can be given by

$$v_{cvdq,ref} = G_{\rm cc} i_{Ldq,ref} - (G_{\rm cc} + G_{\rm del}) i_{L,dq} + v_{o,dq} \quad (4)$$

and defined

$$G_{\rm cc} = \begin{pmatrix} H_{\rm cc}(s) & 0 \\ 0 & H_{\rm cc}(s) \end{pmatrix}$$

$$G_{\rm del} = \begin{pmatrix} 0 & \omega_{\rm PLL} L_c \\ -\omega_{\rm PLL} L_c & 0 \end{pmatrix}$$

where $i_{Ldq,ref} = \begin{pmatrix} i_{Ld,ref} & i_{Lq,ref} \end{pmatrix}^T$; $i_{Ld,ref}$ and $i_{Lq,ref}$ are the reference active and reactive current components obtained from the outer-loop controller of the VSCs; $H_{\rm cc}(s) = k_{\rm pc} + k_{\rm ic}/s$ is the current compensator transfer function, where $k_{\rm pc}$ and $k_{\rm ic}$ are the proportional and the integral gain of the current compensator, respectively; and $\omega_{\rm PLL}$ is the frequency of the phase-locked loop (PLL) in p.u. The analytical modeling of the current controller remains the same for both VSC-A and VSC-B.

B. Power-Controlled Converter—VSC-A

VSC-A controls the active power. The outer-loop PI controller gives the d-axis current reference and the q-axis current reference is set to a constant value according to the reactive power requirements; in this case, it is zero. The control structure of the power-controlled converter is shown in Fig. 3. The current reference for the active power controller can be defined by

$$i_{Ld,ref} = H_p(s)(P_{\rm ref} - P_{\rm meas}) \quad (5)$$

and the measured power

$$P_{\rm meas} = v_{\rm odA} i_{\rm LdA} + v_{\rm oqA} i_{\rm LqA} \quad (6)$$

where $H_p(s) = k_{\rm pp} + k_{\rm ip}/s$ is the power compensator transfer function, where $k_{\rm pp}$ and $k_{\rm ip}$ are the proportional and integral gain of the power controller, respectively. The subscript "A" denotes VSC-A.

C. DC-Voltage-Controlled Converter—VSC-B

The control structure of VSC-B is shown in Fig. 4. VSC-B regulates the HVDC link voltage. The outer-loop PI controller gives the d-axis current reference to the current controller. The q-axis current is set to a constant value. The d-axis current reference $i_{Ld,refB}$ can be given by

$$i_{Ld,refB} = H_{vdc}(s)(v_{dc,refB} - v_{\rm dcB})(-1) \quad (7)$$

where $H_{v\rm dc}(s) = k_{pv\rm dc} + k_{iv\rm dc}/s$ is the dc voltage controller transfer function; k_{pvdc} and k_{ivdc} are the proportional and integral gain of the PI controller, respectively; and $V_{dc,refB}$ is the reference dc voltage. The subscript "B" denotes VSC-B.

III. Simulation and Experiments

The analytical model of a two-terminal VSC-HVDC system discussed in previous section is implemented in MATLAB/Simulink with a detailed switching model of the VSCs. In addition, the simulation results are also compared with the setup of a two-terminal system built in the laboratory. The theoretical analysis and simulations have been performed for a low voltage level in order to compare with the same voltage and system parameters in the experiments. The electrical circuit parameters of the system are given in Table I in the Appendix. The inner-loop current controller of VSC-A is tuned at $H_{\rm ccA}(s) = 4 + 800/{\rm s}$ and the closed-loop control bandwidth is 160 Hz with 150° phase margin. The active power compensator transfer function is $H_P(s) = 0.005 + 1/{\rm s}$, and the closed-loop control bandwidth is 27 Hz with 75° phase margin. The current compensator of VSC-B is $H_{\rm ccB}(s) = 5 + 1000/{\rm s}$ and the closed-loop control bandwidth is 157 Hz with 150° phase margin, and the dc voltage compensator transfer function is $H_{vdc}(s) = 4.5 + 3/{\rm s}$ and the control bandwidth 8 Hz with 170° phase margin. The control tunings satisfy the standard bandwidth requirements and the system is expected to operate stably.

The dc voltage reference to VSC-B is set to 500 V. The active power reference to VSC-A is set to −10 kW. The negative power reference to VSC-A means that VSC-A is exporting active power to the dc system and is operating as a rectifier. Thus, VSC-B is extracting power from the dc system and operates as an inverter. A time-domain simulation has been carried out for these tuning and setting, and the resulting time-domain responses are shown in Figs. 5 and 6, which show that the system operates stably. Fig. 7 shows the experimental results. The system operates stably in both the time-domain simulation and the experiment.

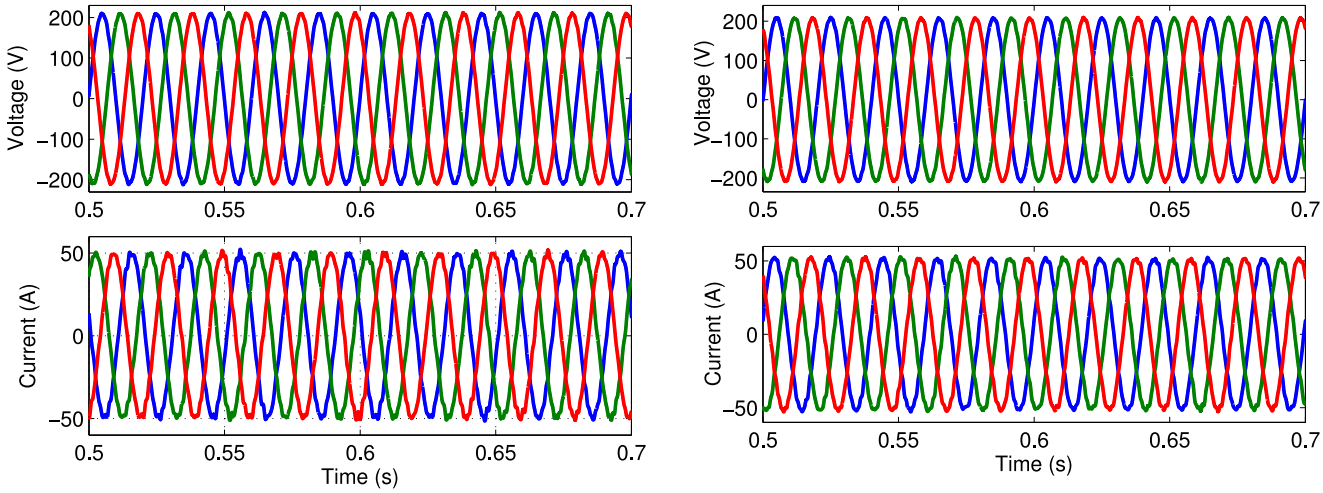

Fig. 5. Simulation results for −10-kW power reference to the VSC-A (stable case). (a) Three-phase ac voltages and currents at PCC of VSC-A. (b) Three-phase ac voltages and currents at PCC of VSC-B of the HVDC system.

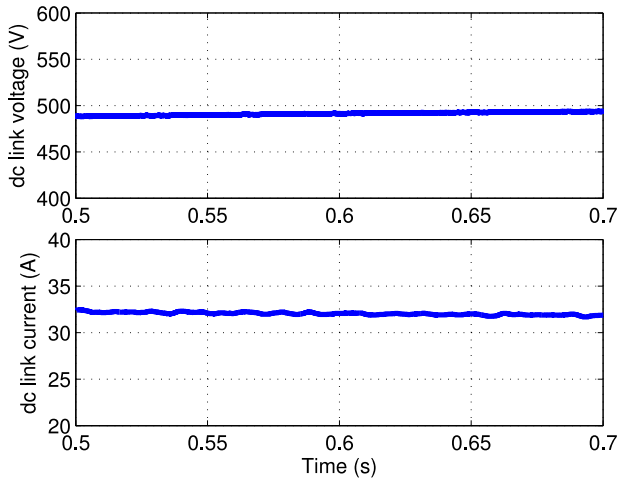

Fig. 6. DC-link voltage and current of the VSC HVDC system.

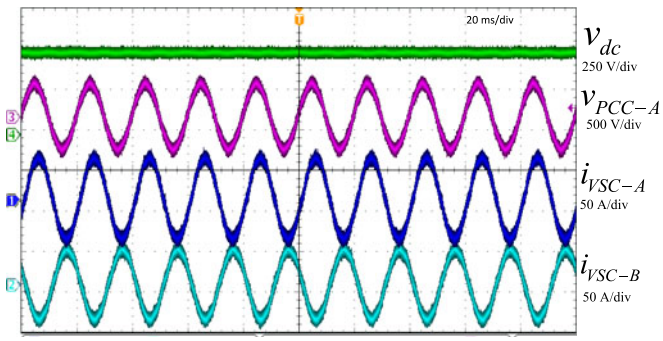

Fig. 7. Experimental results for −10-kW power reference to the VSC-A (stable case). 1) the dc-link voltage, 2) voltage at PCC of VSC (phase-A), 3) current of VSC-A (phase-A), and 4) current of VSC-B (phase-A).

The HVDC system is expected to operate stably for both directions of the power flow. Therefore, the opposite direction of the power flow is tested for the same control tuning. The active power reference is now set to +10 kW, which is the opposite to the previous direction. For this power reference, VSC-A is extracting the power from the dc system and operates as an inverter and VSC-B is exporting power to the dc system. The power reference has been altered from the negative reference to the positive, while the controls of the VSCs remain the same. A time-domain simulation has been carried out, and the resulting time-domain responses are shown in Fig. 8. As can be seen in Fig. 8, the system has become unstable, and the PCC voltage and current are polluted by different harmonic and the dc-link voltage and current have also different frequency of oscillation. An experiment has been carried out for the same setup and power reference. Fig. 9 shows the results from the experiment. The experimental result has confirmed that the system is unstable and has polluted by the different harmonic. Moreover, the operation in the experiment cannot be continued, since protection system has been tripped.

The system operates stably when the power flow direction is from the power-controlled converter to the dc-voltage-controlled converter and becomes unstable when the power flow direction has been altered. To analyze the stability and find the causes of this instability, an impedance-based stability method is adopted. The next two sections have presented the stability analysis of the system and the possible solution to overcome this instability.

IV. Stability Analysis

A. Impedance Modeling and Verification

In order to apply the impedance-based stability method, deriving the impedance model is prerequisite. The stability of the system is analyzed based on the dc impedance. A dc impedance model is derived for a switching model of the VSC including the pulse width modulation (PWM) delay based on the method presented in [24]. The details impedance model derivation is described below.

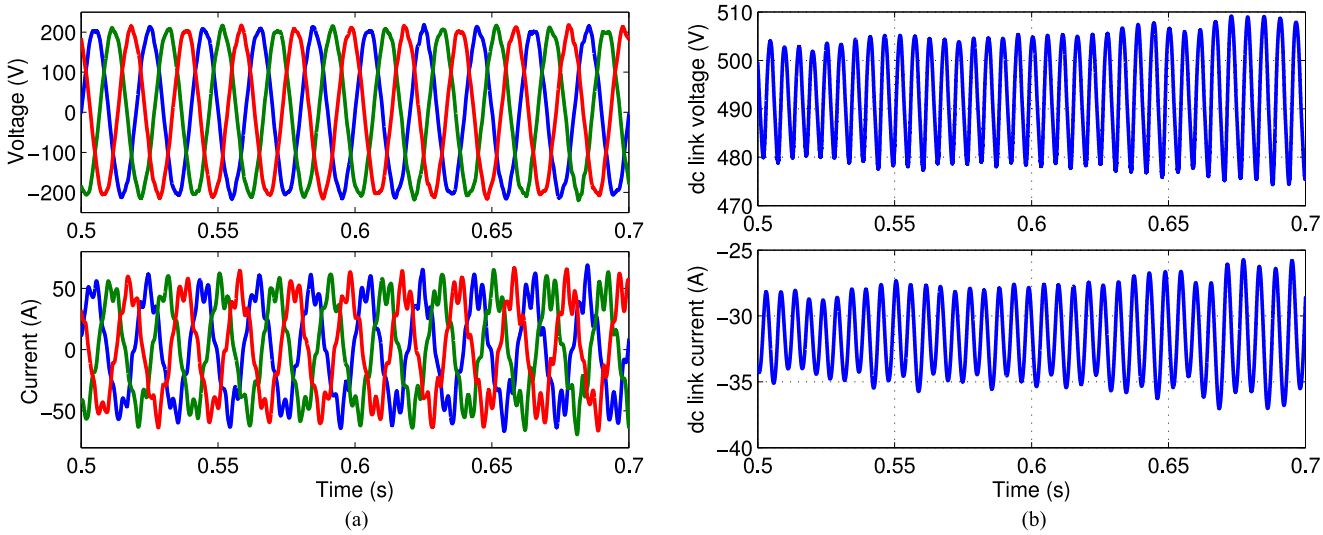

Fig. 8. Simulation results for +10-kW power reference to the VSC-A (unstable case). (a) Three-phase ac voltages and currents at PCC of VSC-B. (b) DC-link voltage and current of the VSC HVDC system.

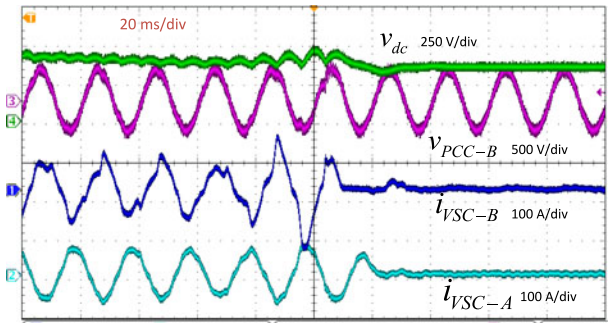

Fig. 9. Experimental results for +10-kW power reference to the VSC-A (unstable case): 1) the dc-link voltage, 2) voltage at PCC of VSC (phase-A), 3) current of VSC-A (phase-A), and 4) current of VSC-B (phase-A).

The impedance model will be derived based on the analytical model of the VSC-HVDC system described in Section II. Applying the small-signal deviation and Laplace transformation and letting $\Delta v_{cv,dq} = \begin{pmatrix} \Delta v_{\rm cvd} & \Delta v_{\rm cvq} \end{pmatrix}^T$, $\Delta v_{o,dq} = \begin{pmatrix} \Delta v_{\rm od} & \Delta v_{\rm oq} \end{pmatrix}^T$, and $\Delta i_{L,dq} = \begin{pmatrix} \Delta i_{\rm Ld} & \Delta i_{\rm Lq} \end{pmatrix}^T$, (1) can be written in matrix form by

$$\Delta v_{cv,dq} = \Delta v_{o,dq} + Z_c \Delta i_{L,dq} \tag{8}$$

where

$$Z_c = \begin{pmatrix} R_c + sL_c/\omega_b & -\omega_g L_c \\ \omega_g L_c & R_c + sL_c/\omega_b \end{pmatrix}.$$

Assuming that the grid voltage v_g is stable and $\Delta v_{g,dq} = 0$, (3) gives the relation between $\Delta i_{o,dq}$ and $\Delta v_{o,dq}$ and can be given by

$$\Delta i_{o,dq} = Y_g \Delta v_{o,dq} \tag{9}$$

where

$$Y_g = \begin{pmatrix} R_g + sL_g/\omega_b & -\omega_g L_g \\ \omega_g L_g & R_g + sL_g/\omega_b \end{pmatrix}^{-1}$$

and $\Delta i_{o,dq} = \begin{pmatrix} \Delta i_{\rm od} & \Delta i_{\rm oq} \end{pmatrix}^T$. The relation between the PCC voltage $\Delta v_{o,dq}$ and converter current $\Delta i_{L,dq}$ can be found by applying Laplace transformation, linearization, and inserting (9) into (2) and can be written by

$$\Delta v_{o,dq} = \overbrace{(Y_{\rm Cf} + Y_g)^{-1}}^{\Omega_g} \Delta i_{L,dq} \tag{10}$$

where

$$Y_{\rm Cf} = \begin{pmatrix} sC_f/\omega_b & -\omega_g C_f \\ \omega_g C & sC_f/\omega_b \end{pmatrix}.$$

Inserting (10) into (8) gives the relation between converter ac voltage $v_{\rm cvdq}$ and ac current $i_{\rm Ldq}$ and can be expressed by

$$\Delta v_{cv,dq} = (\Omega_g + Z_c)\Delta i_{L,dq}. \tag{11}$$

Throughout this paper, it is assumed that the PLL is operating satisfactory and we neglect the impacts of the PLL dynamics. Now applying small-signal deviation and neglecting the higher order term, (4) with small perturbations with $v_{cvdq,ref} = V_{\rm dc,0}(v_{\rm cvdq}/v_{\rm dc})$ can be written by

$$G_{\rm PWM} G_{\rm cc} \Delta i_{dq,ref} = (Z_c + G_{\rm PWM}(G_{\rm cc} + G_{\rm del}))\,\Delta i_{L,dq} - \begin{pmatrix} m_{d0} & m_{q0} \end{pmatrix}^T \Delta v_{\rm dc} \tag{12}$$

where $m_{dq0} = V_{cvdq0}/V_{\rm dc0}$ is the modulation index at an operating point and the PWM delay is modeled as

$$G_{\rm PWM} = \frac{1}{1 + 1.5 T_{\rm sw} s}$$

where $T_{\rm sw} = 1/f_{\rm sw}$; $f_{\rm sw}$ is the switching frequency. If the converter is assumed to have only the current controller, $\Delta i_{Ldq,ref}$ will be zero.

By neglecting the losses due to switching, the power balance constraint between the dc and the ac side can be given by (13)

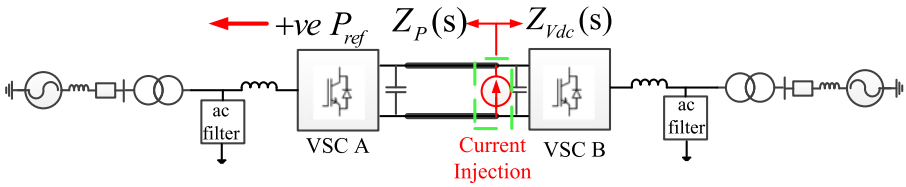

Fig. 10. Investigated point-to-point VSC-based HVDC system including current injection structure for impedance model verification.

and linearized equation of (13) is given by (14):

$$P = v_{\rm dc} i_{\rm dc} = i_{\rm Ld} v_{\rm cvd} + i_{\rm Lq} v_{\rm cvq} \tag{13}$$

$$\begin{pmatrix} I_{\rm dc0} \\ V_{\rm dc0} \end{pmatrix}^T \begin{pmatrix} \Delta v_{\rm dc} \\ \Delta i_{\rm dc} \end{pmatrix} = \begin{pmatrix} I_{Ld0} \\ I_{Lq0} \end{pmatrix}^T \Delta v_{cv,dq} + \begin{pmatrix} V_{cvd0} \\ V_{cvq0} \end{pmatrix}^T \Delta i_{\rm Ldq}. \tag{14}$$

The dc impedance of the converters can be calculated as $\Delta v_{\rm dc}/\Delta i_{\rm dc}$. In (14), the variables $\Delta v_{cv,dq}$ and $\Delta i_{\rm Ldq}$ are ac-side quantities, which imply that the derivation should involve both ac and dc side [35]; therefore, the ac-side quantities have to be expressed in terms of the dc-side quantities in order to get an expression of the dc impedance: $Z_{\rm dc} = \Delta v_{\rm dc}/\Delta i_{\rm dc}$.

Equation (14) can be simplified by inserting (11) as

$$\begin{pmatrix} I_{\rm dc0} \\ V_{\rm dc0} \end{pmatrix}^T \begin{pmatrix} \Delta v_{\rm dc} \\ \Delta i_{\rm dc} \end{pmatrix} = \left(\begin{pmatrix} I_{Ld0} \\ I_{Lq0} \end{pmatrix}^T (\Omega_g + Z_c) \right) \Delta i_{\rm Ldq} + \begin{pmatrix} V_{cvd0} & V_{cvq0} \end{pmatrix} \Delta i_{\rm Ldq} \tag{15}$$

To get the expression of the dc impedance, the ac quantity $\Delta i_{\rm Ldq}$ of (15) have to be expressed with the dc quantity by the dc voltage or the dc current. The investigated HVDC system has the outer-loop active power control in VSC-A and outer-loop dc voltage control in VSC-B. Hence, it is necessary to find an expression of $\Delta i_{Ldq,ref}$ in terms of either $\Delta i_{\rm Ldq}$ or $\Delta v_{\rm dc}$ in (12) to include the impact of the outer loop on the stability.

1) Impedance Model of the Power Controlled-Converter (VSC-A): The analytical modeling of the control of VSC-A is presented in Section II and the impedance modeling of the VSC-A including the outer loop is presented in the following subsection. The reference current $\Delta i_{dq,refA}$ can be obtained in terms of $\Delta i_{\rm LdqA}$ by linearizing (5) and (6) and inserting (10) and rearranging (12) and can be given by

$$\Delta i_{Ldq,refA} = \overbrace{(-G_{\rm iA} - G_{\rm vA}\Omega_g)}^{G_A} \Delta i_{\rm Ldq} \tag{16}$$

where

$$G_{\rm vA} = H_P(s) \begin{pmatrix} V_{od0A} & V_{oq0A} \\ 0 & 0 \end{pmatrix}$$

$$G_{\rm iA} = H_P(s) \begin{pmatrix} I_{Ld0A} & I_{Lq0A} \\ 0 & 0 \end{pmatrix}.$$

Inserting (16) into (12) and solving together with (15), the dc impedance of VSC-A is obtained as

$$Z_{\rm dcA} = \frac{\Delta v_{\rm dcA}}{\Delta i_{\rm dcA}} = \frac{-V_{\rm dc0A}}{I_{\rm dc0A} - k_A G_{idcA}} \tag{17}$$

where

$$k_A = \begin{pmatrix} I_{Ld0A} \\ I_{Lq0A} \end{pmatrix}^T ({Y_{\rm Cf}}^{-1} + Z_g + Z_c) + \begin{pmatrix} V_{cvd0A} \\ V_{cvq0A} \end{pmatrix}^T$$

$$G_{idcA} = (Z_c + G_{\rm PWM}(G_{\rm cc} + G_{\rm del} - G_{\rm cc}G_A))^{-1} \begin{pmatrix} m_{d0A} \\ m_{q0A} \end{pmatrix}.$$

2) Impedance Model of the DC-Voltage-Controlled Converter (VSC-B): The impedance model of the dc-voltage-controlled converter is described in this subsection. The current reference $\Delta i_{Ldq,refB}$ can be expressed in terms of the dc voltage by linearizing (7) and can be given by

$$\Delta i_{Ldq,refB} = \begin{pmatrix} H_{vdc}(s) \\ 0 \end{pmatrix} \Delta v_{\rm dcB}. \tag{18}$$

Inserting (18) into (12) gives the relation between the dc voltage $\Delta v_{\rm dcB}$ and ac currents $\Delta i_{\rm Ldq}$. Now solving (12), (15), and (18) together and rearranging, the dc impedance model of VSC-B can be obtained and is given by

$$Z_{\rm dcB} = \frac{\Delta v_{\rm dcB}}{\Delta i_{\rm dcB}} = \frac{-V_{\rm dc0B}}{I_{\rm dc0B} - k_B G_{idcB}} \tag{19}$$

where

$$k_B = \begin{pmatrix} I_{Ld0B} \\ I_{Lq0B} \end{pmatrix}^T ({Y_{\rm Cf}}^{-1} + Z_g + Z_c) + \begin{pmatrix} V_{cvd0B} \\ V_{cvq0B} \end{pmatrix}^T$$

$$G_{idcB} = (Z_c + G_{\rm PWM}(G_{\rm cc} + G_{\rm del}))^{-1} \times \left(\begin{pmatrix} m_{d0B} \\ m_{q0B} \end{pmatrix} + G_{\rm cc} \begin{pmatrix} H_{V\,dc}(s) \\ 0 \end{pmatrix} \right).$$

B. Stability Analysis Based on the Literature

The investigated two-terminal VSC-HVDC system including the shunt current injection structure for the impedance model verification is depicted in Fig. 10. For stability analysis, the equivalent small-signal impedance model of the VSC-HVDC system is shown in Fig. 11. The power-controlled converter subsystem including the dc-line impedance is modeled by its Norton equivalent circuit consisting of an ideal current source I_P in parallel with equivalent impedance $Z_P(s)$, while the dc-voltage-controlled converter subsystem is modeled by its Thevenin equivalent consisting of a voltage source with a series equivalent impedance $Z_{V\,dc}(s)$.

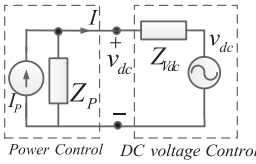

Fig. 11. Equivalent small-signal impedance model of VSC-HVDC system consisting of both the voltage source and the current source.

The current-source impedance can be given by

$$Z_P(s) = \frac{Z_{\mathrm{dcA}}(s)}{1 + sC_{\mathrm{dcA}} Z_{\mathrm{dcA}}(s)} + Z_{dc,cable}(s) \tag{20}$$

and the voltage-source impedance is

$$Z_{V\,dc}(s) = \frac{Z_{\mathrm{dcB}}(s)}{1 + sC_{\mathrm{dcB}} Z_{\mathrm{dcB}}(s)}. \tag{21}$$

The analytical impedance model developed for the VSCs in (20) and (21) is validated by simulation with detailed switching model of the VSCs. A perturbation current (1% of rated dc steady-state current) at different frequency from 1 Hz to 1 kHz is injected as shown in Fig. 10 and the voltage is measured. The fast Fourier transformation (FFT) tool from the SimPower System is used to analyze the different frequency voltage and current, and the impedance is calculated by dividing the voltage by current at each frequency. The analytical and simulation impedance is shown in Fig. 12, and the electrical circuit parameters of this system are given in Table I in the Appendix. The solid line is the analytical impedance and the red points show the results from detailed simulation. Both analytical and simulation impedance magnitude and phase have good agreement, which validates correctness of the impedance model derivation.

The equivalent small-signal impedance model of the VSC-HVDC shown in Fig. 11 is a hybrid system consisting of both a voltage source and a current source. Therefore, the dc voltage at interconnection of Fig. 11 can be given by

$$v(s) = \left(v_{\mathrm{dc}}(s) + i_P(s) Z_{vdc}(s)\right) \frac{1}{1 + \frac{Z_{V\,dc}(s)}{Z_P(s)}} \tag{22}$$

where the second part of the equation resembles a closed-loop transfer function and the stability of the system can be determined by checking the Nyquist plot of the voltage-source to the current-source impedance ratio regardless of the current source behaves as a source or a sink. Moreover, this criterion indicates that a point-to-point connection VSC-HVDC system should be designed to have high output impedance as possible in the current-source subsystem and low input impedance in the voltage source in order to operate stable under a wide range of frequencies.

Fig. 13(a) shows the impedance frequency response of the voltage-source and the current-source subsystem for the negative power reference of the power-controlled converter. As can be seen, the impedance of the current-source subsystem ($Z_P(s)$) is higher than the impedance of the voltage-source subsystem ($Z_{V\,dc}(s)$) at all frequencies, which is desirable to have the stable system. Fig. 13(b) shows the Nyquist plot of the impedance

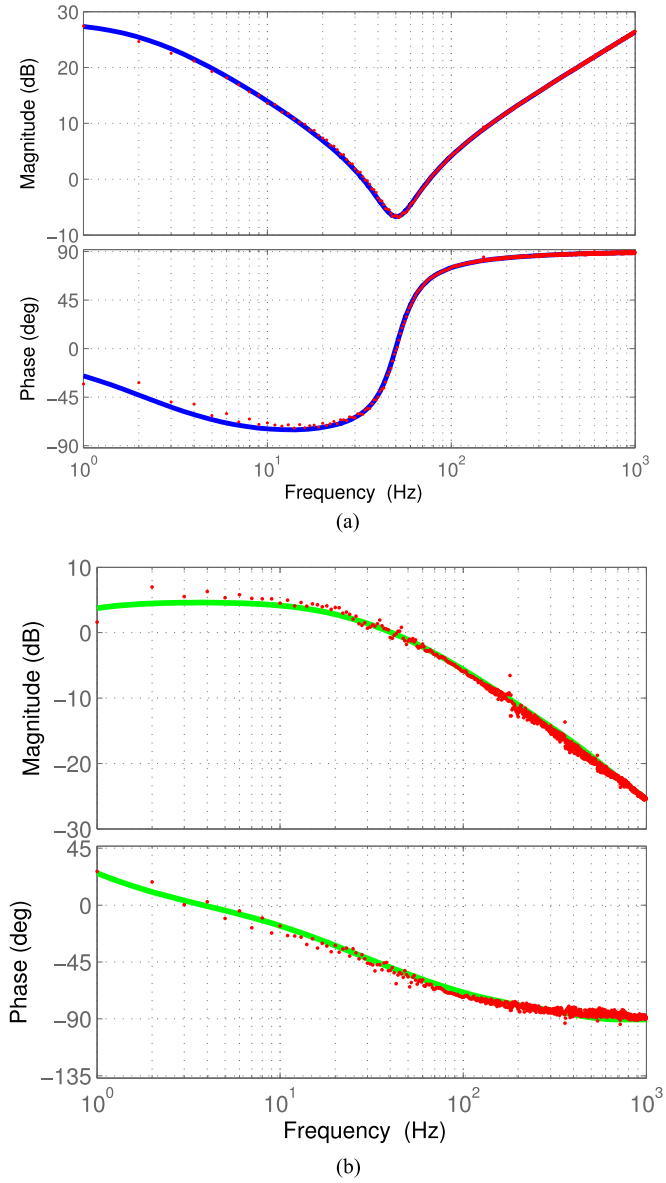

Fig. 12. Frequency response of the impedance. (a) Impedance of the current-source subsystem. (b) Impedance of the voltage-source subsystem (solid line is from model prediction and the red points are from detailed simulation).

ratio. Since the magnitude of the $Z_P(s)$ is higher than the magnitude of the $Z_{V\,dc}(s)$ at all frequencies, the Nyquist plot stays inside the unit circle and it never encircles the point $(-1, j0)$; therefore, the system is stable for the negative power reference. The system is found to be stable in time-domain simulation and in the experiment.

Since the impedance also depends on the steady-state operating point, the impedance is calculated for the +10-kW power reference to VSC-A (which is the new operating point). Fig. 14(a) shows the impedance frequency response for the positive (+10 kW) power reference. As can be seen in Fig. 14(a), the impedance of the current-source subsystem ($Z_P(s)$) is higher than the impedance of the voltage-source subsystem ($Z_{V\,dc}(s)$) at all frequencies; therefore, the Nyquist plot of the impedance ratio stays inside the unit circle and it never encircles the point

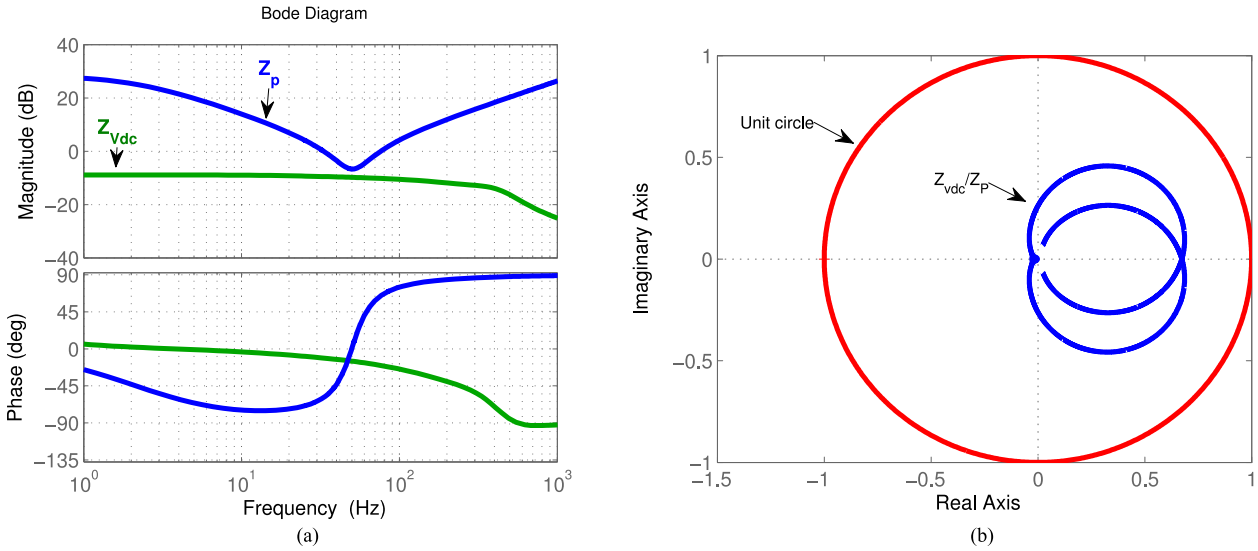

Fig. 13. Negative power reference. (a) Impedance frequency response of the voltage-source and current-source subsystem. (b) Nyquist plot of the impedance ratio $(Z_{V\,dc}(s)/Z_P(s))$.

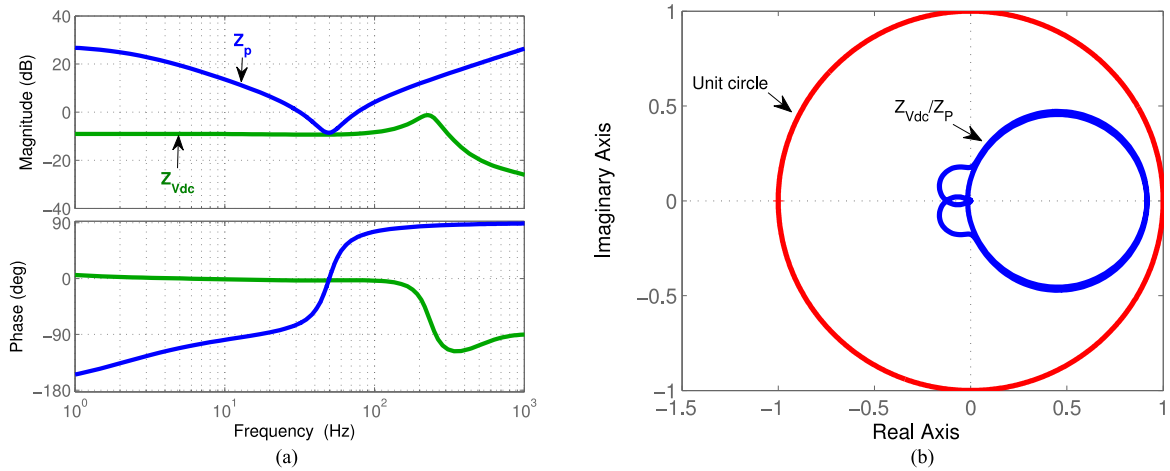

Fig. 14. Positive power reference. (a) Impedance frequency response of the voltage-source and current source subsystem. (b) Nyquist plot of the impedance ratio $(Z_{V\,dc}(s)/Z_P(s))$.

$(-1, j0)$ as shown in Fig. 14(b). Therefore, the system is predicted to be stable from frequency-domain analysis by the existing impedance-based stability method; however, the system is found to be unstable in the time-domain simulation and the experiments. Therefore, the existing method cannot determine the stability of the system when the power flow direction has been altered.

V. Proposed Stability Analysis Method

In previous section, it has been observed that the existing impedance-based method cannot determine the stability of the system when the power flow direction has been altered. Therefore, to overcome this limitation in this paper, an impedance-based stability method is proposed where the subsystems are represented by only a Norton equivalent current source instead of representing them by a hybrid system consisting of both a voltage source and a current source. This assumption is valid, since the voltage-controlled subsystem can be represented by its Norton equivalent current source with parallel connected impedance [20]. The modified equivalent small-signal impedance model of the two-terminal HVDC system is shown in Fig. 15.

Now, we assume that the power reference of the power-controlled converter, VSC-A, is negative; this means that VSC-A injects power into the dc system and works as a current source and the dc-voltage-controlled converter, VSC-B, operates as an inverter and extracts active power from the dc system. Therefore, VSC-A operates as a current source, while VSC-B is a current sink or load. For this condition, the current $I(s)$ at interconnection in Fig. 15 can be given by

$$I(s) = \left(I_P(s) - I_V(s) \frac{Z_{V\,dc}(s)}{Z_P(s)} \right) \frac{1}{1 + \frac{Z_{V\,dc}(s)}{Z_P(s)}}. \qquad (23)$$

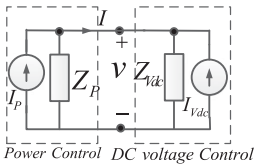

Fig. 15. Equivalent small-signal impedance model of VSC-HVDC system: current-source equivalent model.

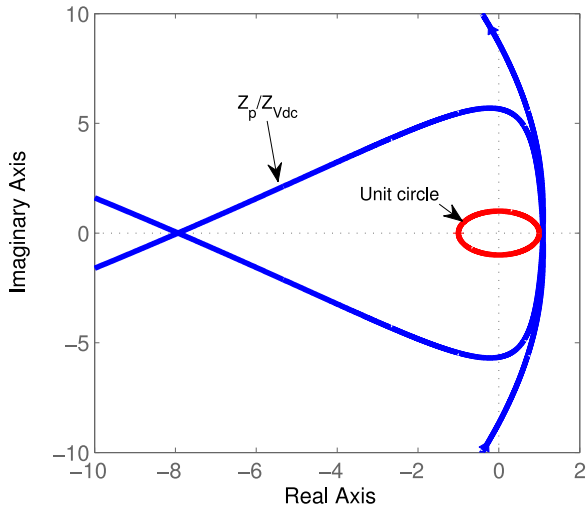

Fig. 16. Nyquist plot of impedance ratio $Z_P(s)/Z_{V\,dc}(s)$.

Note that the second part of (23) resembles the closed-loop transfer function of a negative feedback control system with a forward gain of unity and the feedback gain is $Z_{V\,dc}(s)/Z_P(s)$. Hence, based on (23), the HVDC system will operate stably if the ratio of the dc-voltage-controlled converter impedance to the power-controlled converter impedance $Z_{V\,dc}(s)/Z_P(s)$ satisfies the Nyquist stability criteria. Fig. 13 shows the impedance frequency response and the Nyquist plot of the impedance ratio for the negative power reference and the system is predicted to be stable. The system operates stably in the time-domain simulation and the experiments as shown in Figs. 5 and 7, respectively.

Now, the reference power of VSC-A is set to +10 kW, this means that VSC-A is extracting power from the dc system and working as a current sink or load, while VSC-B is working as a current source. In that case, the current $I(s)$ at interconnection can be given by

$$I(s) = \left(I_V(s) - I_P(s)\frac{Z_P(s)}{Z_{V\,dc}(s)}\right)\frac{1}{1+\frac{Z_P(s)}{Z_{V\,dc}(s)}}. \qquad (24)$$

Therefore, based on (24), the stability of the HVDC system depends on the impedance ratio of the input impedance of the power-controlled subsystem to the output impedance of the dc-voltage-controlled subsystem $Z_P(s)/Z_{V\,dc}(s)$, which is the inverse of the previous assumption of (23). The system operates stably if $Z_P(s)/Z_{V\,dc}(s)$ satisfies the Nyquist stability criteria.

Fig. 16 shows the Nyquist plot of the impedance ratio $Z_P(s)/Z_{V\,dc}(s)$ for the positive power reference of VSC-A. As can be seen in Fig. 14, the magnitude of the $Z_P(s)$ is higher

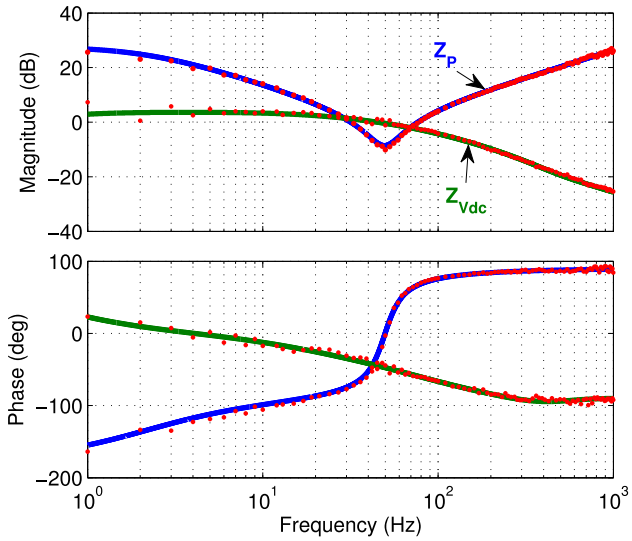

Fig. 17. Frequency response of the impedance model at interfacing point for modified control tuning (the solid line is from model prediction and the red points are from detailed simulation).

than the magnitude of the $Z_{V\,dc}(s)$ and the Nyquist plot of $Z_P(s)/Z_{V\,dc}(s)$ (see Fig. 16) does not cross the unit circle; however, it encircles the point $(-1, j0)$; hence, the system is predicted to be unstable. Therefore, the system has become unstable in the simulation and experiments, as shown in Figs. 8 and 9, respectively.

Equation (24) indicates that the system stability can be improved by increasing the magnitude of $Z_{V\,dc}(s)$, which can be done by modifying the converter passive components and the controller bandwidth. It is not a feasible way to modify the passive components; instead, it is better to modify the controller gain.

Hence, the voltage controller gain is retuned at $H_{V\,dc}(s) = 1 + 3/s$ and the closed-loop crossover frequency is 7.2 Hz with 172° phase margin. Fig. 17 shows the impedance frequency response of the subsystems for the negative power reference. The impedance magnitude crosses each other at frequency of 30.6 and 65.8 Hz with a phase margin of 160° and 66.5°, respectively. Fig. 18 depicts the Nyquist plot of impedance ratio $Z_{V\,dc}(s)/Z_P(s)$. As can be seen in Fig. 18(a), the Nyquist plot does not encircle the point $(-1, j0)$. Therefore, it has been predicted that the system operates stably for the negative power reference. Now, stability analysis is performed for the positive power reference, and the resulting Nyquist plot of the impedance ratio $Z_P(s)/Z_{\mathrm{V\,dc}}(s)$ is shown in Fig. 18(b) and the Nyquist plot predicts that the system will operate stably. The system is predicted to be stable for both directions of the power flow.

A time-domain simulation has been carried out for a step of active power reference from −10 to +10 kW and the resulting time-domain simulation is shown in Fig. 19. The system operates stably for both directions of power flow, which is further confirmed in the experiments. Both the simulation and the experiments have validated the theoretical analysis.

Moreover, the impact of the controller dynamics on the stability has been investigated to further validate the effectiveness

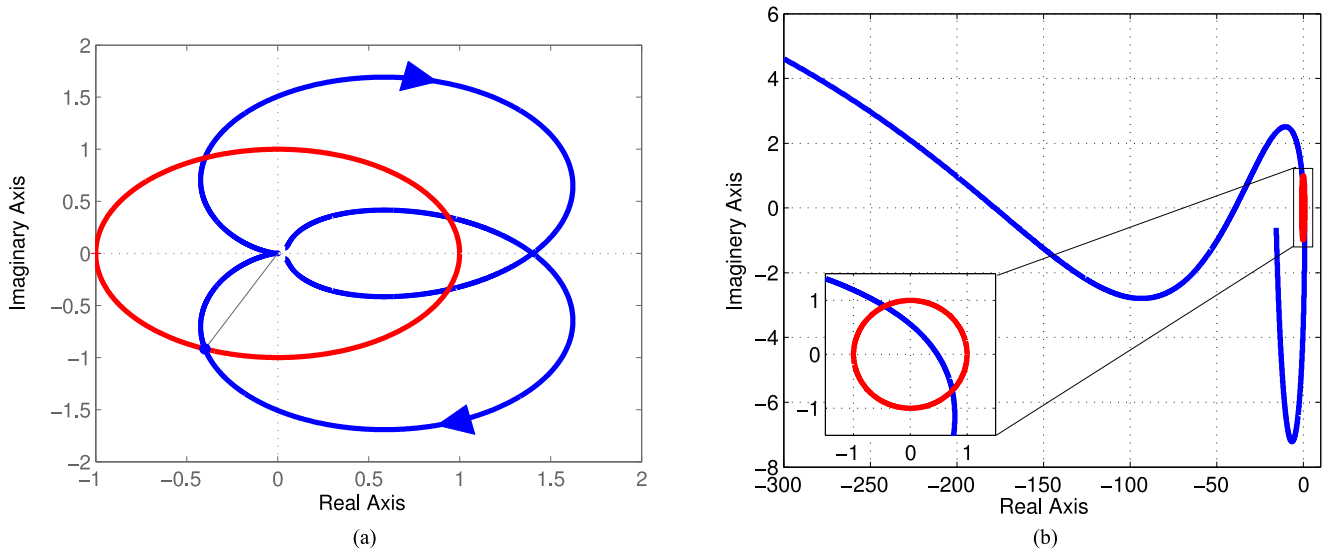

Fig. 18. Nyquist plot of impedance ratio for modified control tuning. (a) Negative power reference: $Z_{V\,dc}(s)/Z_P(s)$. (b) Positive power reference: $Z_P(s)/Z_{V\,dc}(s)$.

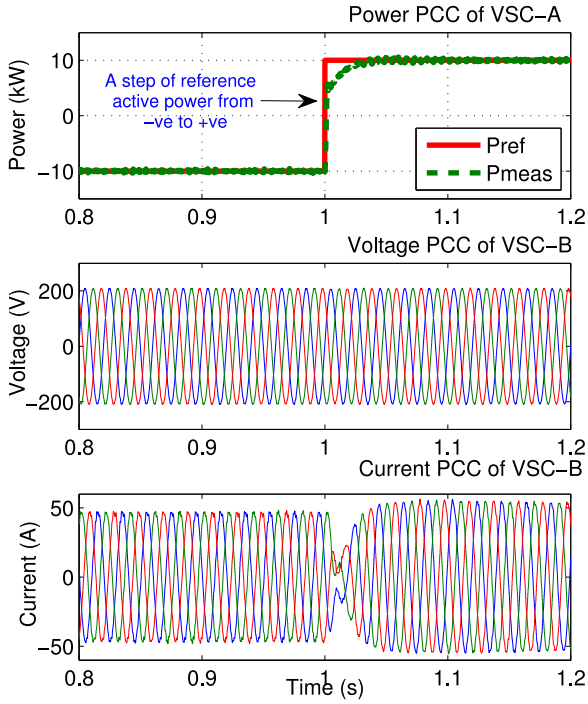

Fig. 19. Simulation results for a step change of power reference from negative to positive 10 kW.

of the dc-impedance-based method. The proportional gain of the dc voltage controller further reduces to 0.03 with the closed-loop crossover frequency of 7.13 Hz and 148° phase margin. The impedance frequency response and the Nyquist plot for this tuning is shown in Fig. 20. As can be seen in Fig. 20(a), the dc-voltage-controlled subsystem impedance becomes larger at low frequency for lower value of proportional gain, and it crosses the unit circle at frequency of 2.96 Hz with low phase margin (20°) as shown in Fig. 20(b). Since Nyquist plot does not encircle the point $(-1, j0)$, the system is stable. However, the phase margin is low, the system would have a low-frequency oscillation at around 2.96 Hz in transient condition.

A time-domain simulation has been carried out and the time-domain response of the dc voltage and the current and FFT of the dc current are shown in Fig. 21(a). As can be seen, the system has a stable pole with oscillation frequency around 3 Hz as predicted in the frequency-domain analysis by the Nyquist plot in Fig. 20(b). This oscillation is also observed in the ac side as shown in Fig. 21(b), which is reflected by 50-Hz fundamental frequency f_1 as $\pm(f - f_1)$ [27].

An example case is also presented to show the impact of the power controller dynamics on the system stability. The power controller proportional gain is purposely increased to 2×0.005 and the closed-loop crossover frequency is 27 Hz and 116° phase margin. The corresponding impedance frequency response defined in (20) is shown in Fig. 22. As can be seen, the increased gain does not have significant impact on the impedance frequency response. It is because the dc-link capacitance and the dc-line inductance are together behaving as a low-pass filter and the high-frequency oscillations has been filtered by this low-pass filter. Therefore, it cannot predict the instability, which results the high-frequency oscillation from the source and load impedance defined at the interfacing point of Fig. 10. In order to determine instability caused by the power controller dynamics, the impedance-based analysis needs to be performed at the interfacing point as shown in Fig. 23, where the subsystem impedances are defined as

$$Z_P^*(s) = Z_{\mathrm{dcA}}(s) \tag{25}$$

$$Z_{V\,dc}^*(s) = \frac{1}{sC_{\mathrm{dcA}}} \parallel \left(Z_{dc,cable}(s) + \frac{Z_{\mathrm{dcB}}(s)}{1 + sC_{\mathrm{dcB}} Z_{\mathrm{dcB}}(s)} \right). \tag{26}$$

The system is represented by the small-signal equivalent impedance model as depicted in Fig. 15 and the stability is

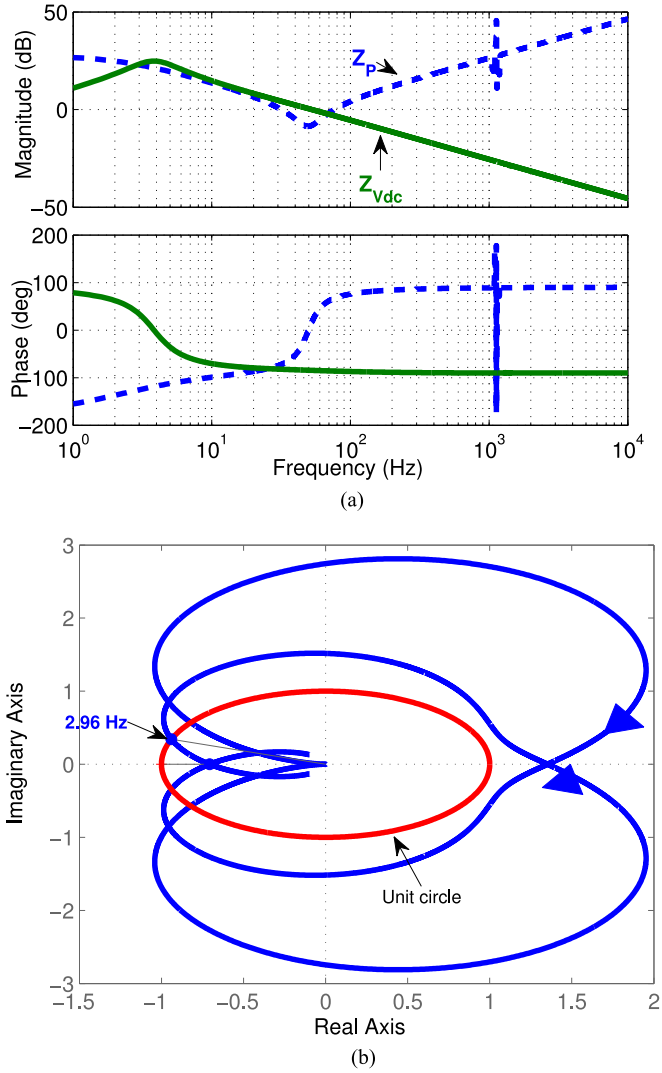

Fig. 20. (a) Impedance of the subsystem for dc voltage control proportional gain of 0.03. (b) Nyquist plot of impedance ratio $Z_{V\,dc}(s)/Z_P(s)$.

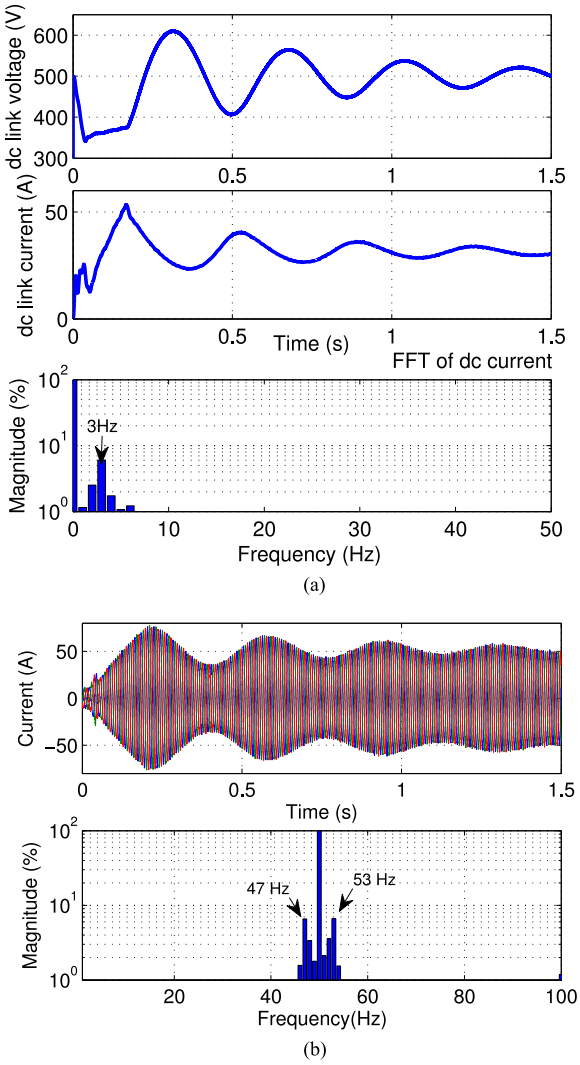

Fig. 21. Simulation results. (a) DC-link voltage and current and FFT of dc current for dc voltage controller proportional gain of 0.03. (b) Three-phase currents at PCC of VSC-B for dc voltage controller proportional gain of 0.03.

predicted by the GNC. The Nyquist plot of $Z^*_{V\,dc}(s)/Z^*_P(s)$ is shown Fig. 24 for two different values of proportional gain of power controller. As can be seen in Fig. 24, the system is stable for $k_{\rm pp} = 0.005$ and unstable for $k_{\rm pp} = 2 \times 0.005$. A time-domain simulation has been carried out to verify the theoretical analysis and the resulting time-domain response is shown in Fig. 25. The proportional gain of the power control has been increased at 0.5 s. As can be seen in Fig. 25, the system operates stably for $k_{\rm pp} = 0.005$ and it introduces harmonic instability for $k_{\rm pp} = 2 \times 0.005$ at 0.5 s. The simulation result is further verified in the experiment. The experimental results are shown in Fig. 26. As can be seen, the system has been polluted by the harmonic oscillation. Both the simulation and experiment results have the harmonic oscillation, which has been predicted from the Nyquist plot of impedance ratio as shown in Fig. 24.

A weakness of the dc-impedance-based method is that it cannot determine the instability that results for a weak network, because variation of the ac grid impedance does not

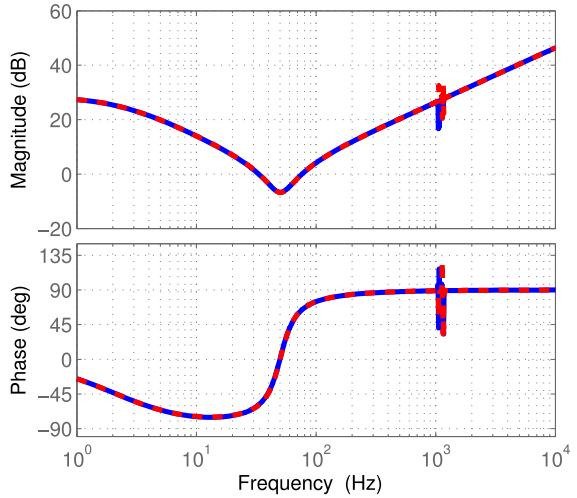

Fig. 22. Impedance frequency response for different values of proportional gain of power controller (solid-blue line is for $k_{\rm pp} = 0.005$ and red-dashed line is for $k_{\rm pp} = 2 \times 0.005$).

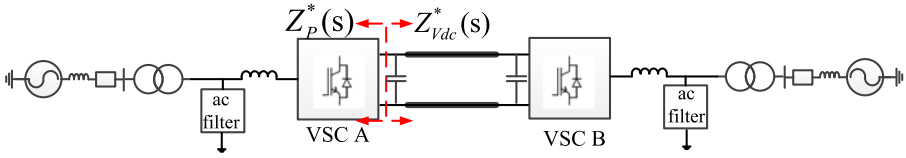

Fig. 23. Point-to-point VSC-based HVDC system to study the impact of power controller dynamics.

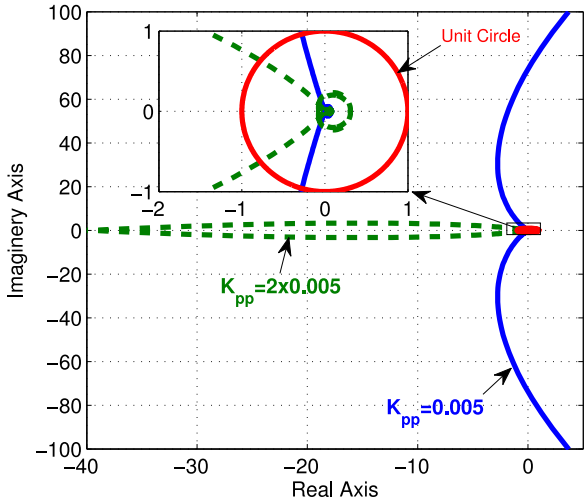

Fig. 24. Nyquist plot of impedance ratio $Z^*_{V\,dc}(s)/Z^*_P(s)$ (blue line is for $k_{\rm pp} = 0.005$ and green-dashed line is for $k_{\rm pp} = 2 \times 0.005$).

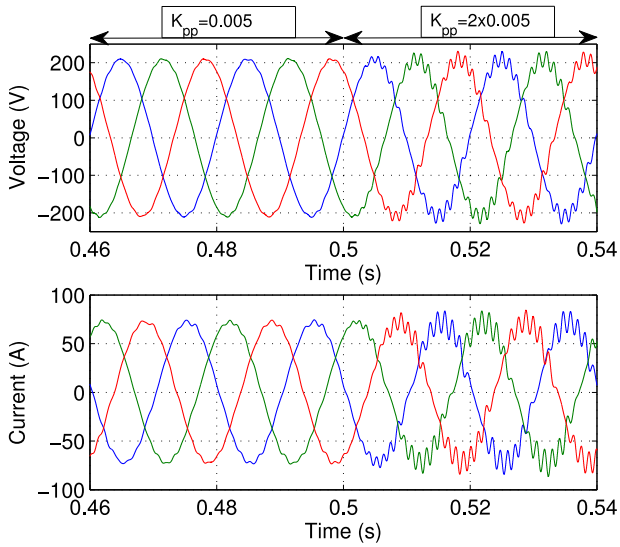

Fig. 25. Three-phase voltages and currents at PCC of VSC-A for a change of the power controller proportional gain from 0.005 to 2×0.005 at 0.5 s.

reflect significantly on the dc impedance [35]. Therefore, the dc-impedance-based analysis is used to analyze the stability in the dc side. On the other hand, the ac-impedance-based analysis cannot determine the instability caused by the dc-line dynamics, since we calculate the ac impedance assuming the dc side a constant voltage source because of large dc-link capacitor. Therefore, to determine the instability resulting for the weak grid/network, the stability analysis should be performed in the ac side based on the ac impedance either in positive–negative sequence impedance [26], [27] or the *dq* frame impedance [28]–[30].

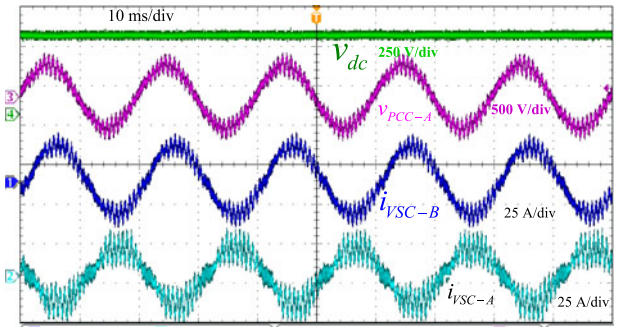

Fig. 26. Experimental results for power controller proportional gain of 2×0.005: 1) dc-link voltage, 2) voltage at PCC of VSC-A (phase-A), current of 3) VSC-B (phase-A) and 4) VSC-A (phase-A).

VI. Conclusion

This paper has presented the impact of the power flow direction on the stability for a two-terminal VSC-HVDC system. It has been observed that the system operates stably when the power flow direction is from the power-controlled converter to the dc-voltage-controlled converter, and it becomes unstable when the power flow direction has been altered. To overcome this problem, an impedance-based method is proposed. The existing method of determining the source and the load impedances cannot predict the stability when the power flow direction has been altered; therefore, a method based on the power flow direction has been presented to determine the source and the load impedance. The converter that is injecting power to the dc system is the current source represented with its Norton equivalent parallel impedance, while the other converter impedance is considered as the load impedance. The stability of the system has been determined by the ratio of the load impedance to the current-source impedance. Once the source and the load impedance are analytically obtained, the impedance-based generalized Nyquist stability criteria have been applied to predict the stability of the interconnected system. The control has been redesigned based on the proposed method such that the power flows in both directions without changing the control between the converters. The system stability for the two power flow directions is well predicted from the Nyquist plot of impedance ratio. A two-terminal HVDC system has been developed in MATLAB/Simulink to demonstrate the application of this method, and the results have been compared with the experimental results.

APPENDIX

TABLE I
INVESTIGATED SYSTEM PARAMETERS

Parameter	Value	Parameter	Value
Rated Power, S_b	150 kVA	L_c	2.1 mH
Rated ac voltage	380 V	R_c	0.01 Ω
Rated frequency	50 Hz	C_f	50 uF
Trans. inductance	0.04 p.u.	V_{dc}	500 V
Trans. resistance	0.005 p.u.	L_{dc}	1.66 mH
Grid inductance	0.1 p.u.	R_{dc}	0.2 Ω
Grid resistance	0.0229 p.u.	C_{dc}	3 mF

REFERENCES

[1] N. Flourentzou, V. G. Agelidis, and G. D. Demetriades, "VSC-based HVDC power transmission systems: An overview," *IEEE Trans. Power Electron.*, vol. 24, no. 3, pp. 592–602, Mar. 2009.

[2] M. P. Bahrman and B. K. Johnson, "The ABCs of HVDC transmission technologies," *IEEE Power Energy Mag.*, vol. 5, no. 2, pp. 32–44, Mar./Apr. 2007.

[3] J. Beerten, S. Cole, and R. Belmans, "Modeling of multi-terminal VSC HVDC systems with distributed DC voltage control," *IEEE Trans. Power Syst.*, vol. 29, no. 1, pp. 34–42, Jan. 2014.

[4] M. Guan and Z. Xu, "Modeling and control of a modular multilevel converter-based HVDC system under unbalanced grid conditions," *IEEE Trans. Power Electron.*, vol. 27, no. 12, pp. 4858–4867, Dec. 2012.

[5] L. Shen, M. Barnes, R. Preece, J. V. Milanovic, K. Bell, and M. Belivanis, "The effect of VSC-HVDC control on AC system electromechanical oscillations and DC system dynamics," *IEEE Trans. Power Del.*, vol. 31, no. 3, pp. 1085–1095, Jun. 2016.

[6] S. Li, T. A. Haskew, and L. Xu, "Control of HVDC light system using conventional and direct current vector control approaches," *IEEE Trans. Power Electron.*, vol. 25, no. 12, pp. 3106–3118, Dec. 2010.

[7] G. Liu, F. Xu, Z. Xu, Z. Zhang and G. Tang, "Assembly HVDC breaker for HVDC grids with modular multilevel converters," *IEEE Trans. Power Electron.*, 2016, to be published.

[8] G. Stamatiou and M. Bongiorno, "Stability analysis of two-terminal VSC-HVDC systems using the net-damping criterion," *IEEE Trans. Power Del.*, 2016, to be published.

[9] M. Guan and Z. Xu, "Modeling and control of a modular multilevel converter-based HVDC system under unbalanced grid conditions," *IEEE Trans. Power Electron.*, vol. 27, no. 12, pp. 4858–4867, Dec. 2012

[10] C. Karawita and U. D. Annakkage, "Multi-infeed HVDC interaction studies using small-signal stability assessment," *IEEE Trans. Power Del.*, vol. 24, no. 2, pp. 910-918, Apr. 2009.

[11] S. Cole, J. Beerten, and R. Belmans, "Generalized dynamic VSC MTDC model for power system stability studies," *IEEE Trans. Power Syst.*, vol. 25, no. 3, pp. 1655–1662, Aug. 2010,

[12] M. K. Zadeh, M. Amin, J. A. Suul, M. Molinas, and O. B. Fosso, "Small-signal stability study of the Cigré DC grid test system with analysis of participation factors and parameter sensitivity of oscillatory modes," in *Proc. Power Syst. Comput. Conf.*, 2014, Wrocław, Poland, 2014, pp. 1–8.

[13] G. O. Kalcon, G. P. Adam, O. Anaya-Lara, S. Lo, and K. Uhlen, "Small-signal stability analysis of multi-terminal VSC-based DC transmission systems," *IEEE Trans. Power Syst.*, vol. 27, no. 4, pp. 1818–1830, Nov. 2012.

[14] M. Amin, J. A. Suul, S. D'Arco, E. Tedeschi, and M. Molinas, "Impact of state-space modelling fidelity on the small-signal dynamics of VSC-HVDC systems," in *Proc. 11th IET Int. Conf. AC DC Power Transmiss.*, Birmingham, U.K., 2015, pp. 1–11.

[15] Y. Song and C. Breitholtz, "Nyquist stability analysis of an AC-grid connected VSC-HVDC system using a distributed parameter DC cable model," *IEEE Trans. Power Del.*, vol. 31, no. 2, pp. 898–907, Apr. 2016.

[16] G. Pinares and M. Bongiorno, "Modeling and analysis of VSC-based HVDC systems for DC network stability studies," *IEEE Trans. Power Del.*, vol. 31, no. 2, pp. 848–856, Apr. 2016.

[17] J. Beerten, S. D'Arco, and J. A. Suul, "Identification and small-signal analysis of interaction modes in VSC MTDC systems," *IEEE Trans. Power Del.*, vol. 31, no. 2, pp. 888–897, Apr. 2016.

[18] M. Amin, M. Zadeh, J. A. Suul, E. Tedeschi, M. Molinas, and O. B. Fosso, "Stability analysis of interconnected AC power systems with multi-terminal DC grids based on the Cigr DC grid test system," *Proc. 3rd Renewable Power Gener. Conf.*, Naples, Italy, 2014.

[19] R. D. Middlebrook, "Input filter considerations in design and application of switching regulators," in *Proc. Rec. 1976 IEEE Ind. Appl. Soc. Annu. Meet.*, pp. 366–382.

[20] J. Sun, "Impedance-based stability criterion for grid-connected inverters," *IEEE Trans. Power Electron.*, vol. 26, no. 11, pp. 3075–3078, Nov. 2011.

[21] M. Cespedes, L. Xing, and J. Sun, "Constant-power load system stabilization by passive damping," *IEEE Trans. Power Electron.*, vol. 26, no. 7, pp. 1832–1836, Jul. 2011.

[22] H. Liu, S. Shah, and J. Sun, "An impedance-based approach to HVDC system stability analysis and control development," *Proc. 2014 Int. Power Electron. Conf.*, Hiroshima, Japan, 2014, pp. 967–974.

[23] J. Lyu, X. Cai, and M. Molinas, "Frequency domain stability analysis of MMC-based HVdc for wind farm integration," *IEEE J. Emerg. Sel. Topics Power Electron.*, vol. 4, no. 1, pp. 141–151, Mar. 2016.

[24] M. Amin and M. Molinas, "Impedance based stability analysis of VSC-based HVDC system," in *Proc. PowerTech*, Eindhoven, Netherlands, 2015, pp. 1–6.

[25] M. Amin, A. Rygg, and M. Molinas, "Impedance-based and eigenvalue based stability assessment compared in VSC-HVDC system," in *Proc. 8th Annu. IEEE Energy Convers. Congr. Expo.*, Milwaukee, WI, USA, 2016, accepted for publication.

[26] H. Liu and J. Sun, "Voltage stability and control of offshore wind farms with AC collection and HVDC transmission," *IEEE J. Emerg. Sel. Topics Power Electron.*, vol. 2, no. 4, pp. 1181–1189, Dec. 2014.

[27] M. Cespedes and J. Sun, "Impedance modeling and analysis of grid-connected voltage-source converters," *IEEE Trans. Power Electron.*, vol. 29, no. 3, pp. 1254–1261, Mar. 2014.

[28] B. Wen, D. Dong, D. Boroyevich, R. Burgos, P. Mattavelli, and Z. Shen, "Impedance-based analysis of grid-synchronization stability for three-phase paralleled converters," *IEEE Trans. Power Electron.*, vol. 31, no. 1, pp. 26–38, Jan. 2016.

[29] B. Wen, D. Boroyevich, R. Burgos, P. Mattavelli, and Z. Shen, "Inverse Nyquist stability criterion for grid-tied inverters," *IEEE Trans. Power Electron.*, 2016, to be published.

[30] Bo. Wen, D. Boroyevich, R. Burgos, P. Mattavelli, and Z. Shen, "Analysis of D-Q small-signal impedance of grid-tied inverters," *IEEE Trans. Power Electron.*, vol. 31, no. 1, pp. 675–687, Jan. 2016.

[31] S. Lissandron, L. Dalla Santa, P. Mattavelli, and B. Wen, "Experimental validation for impedance-based small-signal stability analysis of single-phase interconnected power systems with grid-feeding inverters," *IEEE J. Emerg. Sel. Topics Power Electron.*, vol. 4, no. 1, pp. 103–115, Mar. 2016.

[32] B. Wen, D. Boroyevich, R. Burgos, P. Mattavelli, and Z. Shen, "Small-signal stability analysis of three-phase AC systems in the presence of constant power loads based on measured d-q frame impedances," *IEEE Trans. Power Electron.*, vol. 30, no. 10, pp. 5952–5963, Oct. 2015.

[33] L. Xu and L. Fan, "Impedance-based resonance analysis in a VSC-HVDC system," *IEEE Trans. Power Del.*, vol. 28, no. 4, pp. 2209–2216, Oct. 2013.

[34] X. Wang, F. Blaabjerg, and W. Wu, "Modeling and analysis of harmonic stability in an AC power-electronics-based power system," *IEEE Trans. Power Electron.*, vol. 29, no. 12, pp. 6421–6432, Dec. 2014.

[35] L. Xu, L. Fan, and Z. Miao, "DC impedance-model-based resonance analysis of a VSC-HVDC system," *IEEE Trans. Power Del.*, vol. 30, no. 3, pp. 1221–1230, Jun. 2015.

[36] M. Amin, A. Rygg, and M. Molinas, "Active power flow direction effect on stability in multi-terminal VSC-HVDC transmission system in integrating wind farm," in *Proc. 2016 IEEE 17th Workshop Control Model. Power Electron.*, Trondheim, Norway, 2016, pp. 1–8.

[37] J. Sun, "Autonomous local control and stability analysis of multiterminal DC systems," *IEEE J. Emerg. Sel. Topics Power Electron.*, vol. 3, no. 4, pp. 1078–1089, Dec. 2015.

[38] V. Blasko and V. Kaura, "A new mathematical model and control of a three-phase AC-DC voltage source converter," *IEEE Trans. Power Electron.*, vol. 12, no. 1, pp. 116–123, Jan. 1997.

[39] N. Kroutikova, C. A. Hernandez-Aramburo, and T. C. Green, "State-space model of grid-connected inverters under current control mode," *IET Electr. Power Appl.*, vol. 1, no. 3, pp. 329–338, May 2007.

Mohammad Amin (M'11) received the B.Sc. degree in electrical and electronic engineering from Chittagong University of Engineering and Technology, Chittagong, Bangladesh, and the M.Sc. degree in electric power engineering from Chalmers University of Technology, Gothenburg, Sweden in 2008 and 2011, respectively. He is working toward the Ph.D. degree at Norwegian University of Science and Technology, Trondheim, Norway.

He was with the Department of Electrical and Electronic Engineering, International Islamic University Chittagong as a Lecture from August 2008 to November 2011 and an Assistant Professor from December 2011 to July 2013. He was a Ph.D. Visiting Scholar at the Wind Power Research Center, Shanghai Jiao Tong University, Shanghai, China, from May 2015 to July 2015. His research interests include stability and interaction analysis in voltage-source-converter- and modular-multilevel-converter-based offshore high-voltage dc system, grid integration of wind farm, control of power converters, and flexible ac transmission systems.

Marta Molinas (M'94) received the Diploma degree in electromechanical engineering from the National University of Asuncion, Asuncion, Paraguay, in 1992, the Master of Engineering degree from Ryukyu University, Nishihara, Japan, in 1997, and the Doctor of Engineering degree from Tokyo Institute of Technology, Tokyo, Japan, in 2000.

She was a Guest Researcher with the University of Padova, Padova, Italy, during 1998. From 2004 to 2007, she was a Postdoctoral Researcher with Norwegian University of Science and Technology (NTNU), and from 2008 to 2014, she was a Professor at the Department of Electric Power Engineering at the same university. She is currently a Professor at the Department of Engineering Cybernetics, NTNU. Her research interests include stability of power electronics systems, harmonics, instantaneous frequency, and nonstationary signals from the human and the machine.

Dr. Molinas is Associate Editor for the IEEE JOURNAL OF EMERGING AND SELECTED TOPICS IN POWER ELECTRONICS and IEEE TRANSACTIONS ON POWER ELECTRONICS and the Editor of the IEEE TRANSACTIONS ON ENERGY CONVERSION. She was an AdCom Member of the IEEE Power Electronics Society from 2009 to 2011.

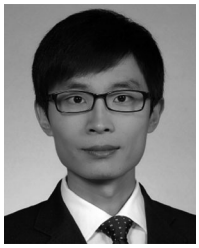

Jing Lyu (S'14) received the B.Eng. degree from China University of Mining and Technology, Jiangsu, China, in 2009, the M.Sc. degree from Shanghai Jiao Tong University, Shanghai, China, in 2011, both in electrical engineering. He is currently working toward the Ph.D. degree in electrical engineering at Shanghai Jiao Tong University.

He was a Ph.D. Visiting Scholar at the Department of Engineering Cybernetics, Norwegian University of Science and Technology, Trondheim, Norway, from January 2015 to March 2015. His research interests include wind energy conversion systems, high-voltage dc technology, modular multilevel converter, and stability in power-electronics-based power systems.

Xu Cai received the B.Eng. degree from Southeast University, Nanjing, China, in 1983, the M.Sc. and Ph.D. degrees from China University of Mining and Technology, Jiangsu, China, in 1988 and 2000, respectively. All are in electrical engineering

He was an Associate Professor with the Department of Electrical Engineering, China University of Mining and Technology, from 1989 to 2001. He joined Shanghai Jiao Tong University, as a professor in 2002, and as the Director of Wind Power Research Center of Shanghai Jiao Tong University in 2008. He was the Vice Director of State Energy Smart Grid R&D Center, Shanghai, China, from 2010 to 2013. His main research interests include power electronics and renewable energy exploitation and utilization, including wind power converters, wind turbine control system, large power battery storage systems, clustering of wind farms, and its control system and grid integration.